# FIELDS AROUND THE STATIC QUARK–ANTIQUARK PAIR IN THE BORN APPROXIMATION ON A LATTICE

T. BARCZYK

Institute of Physics, Jagellonian University
Reymonta 4, 30-059 Cracow, Poland

*(Received January 22, 1993)*

We present the results of the numerical weak coupling calculations of the distribution of the chromoelectric and chromomagnetic field around the static quark-antiquark pair. Comparison with the Monte Carlo data is also performed in an attempt to filter off lowest order perturbative part of the MC results.

PACS numbers: 14.80. Dq

## 1. Introduction

For many years one of the basic questions in lattice research is the problem of confinement. In close connection with it the chromoelectric and chromomagnetic field distribution around static quarks is extensively investigated. First, exploratory study of the problem of energy density distribution using Monte Carlo techniques was done by Fukugita and Niuya [1] for SU(2) and then by Flower and Otto [2] for SU(3). More extensive studies were carried out by Sommer [3, 7]. Distributions around adjoined source were also considered by Jorysz and Michael [6]. Large scale Monte Carlo simulations were performed during 1987–1989 by the Cracow–LSU collaboration [4, 8], giving the shape of the flux tube for large quark separations (up to 9 lattice units).

Here we use the weak coupling expansion method on a lattice to approach the problem. Extracting lowest order perturbative effects will enable us to analyze more precisely MC results in an attempt to understand the influence of nonperturbative phenomena [8]. This work is organized as follows: in Section 2 we obtain formulas which relate color field components to lattice propagators in the weak coupling domain. Section 3 gives some

numerical details and presents the method of computing the correlations between Wilson loops and plaquettes. Section 4 contains the discussion of the results.

## 2. Weak coupling description of the color fields

The connection between lattice observables and the components of the chromoelectric and chromomagnetic field is established by the formula [1, 4]

$$f_{\mu\nu} = \frac{\beta}{a^4} \frac{\langle W P_{\mu\nu}(x)\rangle - \langle W\rangle\langle P_{\mu\nu}(x)\rangle}{\langle W\rangle}, \tag{1}$$

where $W$ denotes the Wilson loop and $P_{\mu\nu}(x)$ the plaquette oriented in plane $\mu\nu$ with the center at $x$.

In the classical continuum limit ($a \to 0$)

$$f_{\mu\nu} \to -\tfrac{1}{2} < F_{\mu\nu}^2 > . \tag{2}$$

So that $-2f_{ik}$ represent squared magnetic components of the color fields and $2f_{i4}$ squared electric ones in the Minkowski space. As we see in order to find the distribution of the field around the static $q\bar{q}$ pair we need to measure the expectation value of the Wilson loop and the correlations between the loop and plaquettes.

The average $\langle W\rangle$ is defined as follows

$$\langle W\rangle = \left\langle \left(\frac{1}{n}\right) \mathrm{Tr} \prod_{l\in W} U_l \right\rangle = \frac{1}{Z} \int [dU] \left(\frac{1}{n}\right) \mathrm{Tr} \prod_{l\in W} U_l e^{A[U]}, \tag{3}$$

where $n$ normalizes the trace and equals 2 for SU(2) , $A[U]$ is the action expressed as

$$A[U] = \beta \sum_{x,\mu>\nu} \mathrm{Re} P_{\mu\nu}(x), \tag{4}$$

and link variables $U_l$ are given by

$$U_l = e^{i g_0 A_l}, \tag{5}$$

where the lattice constant $a$ was absorbed into $A_l$. Defining $g = ig_0$ one can expand the $U_l$

$$U_l = 1 + gA_l + \tfrac{1}{2} g^2 A_l^2 + \cdots . \tag{6}$$

The formula for $\langle W P_{\mu\nu}(x)\rangle$ reads

$$\langle WP_{\mu\nu}(x)\rangle = \left\langle \left(\frac{1}{n}\right) \mathrm{Tr} \prod_{l\in W} U_l \left(\frac{1}{n}\right) \mathrm{Tr} \prod_{l'\in P} U_{l'} \right\rangle . \tag{7}$$

In both cases the key problem is to find the trace of the product of the link variables around the Wilson loop using (6). One can expand the product of the links around the loop in terms of appropriate field components

$$\prod_{l\in W} U_l = 1 + g \sum_{l\in W} A_l + \tfrac{1}{2} g^2 \sum_{l,m\in W} A_l A_m + \tfrac{1}{2} g^2 \sum_{l<m\in W} [A_l, A_m] + O(g^3) . \tag{8}$$

Both linear and commutator terms vanish after applying the trace operation so that (7) can be rewritten in the general form

$$\langle WP_{\mu\nu}(x)\rangle = \left\langle \left(1 + w_2 g^2 + w_3 g^3 + w_4 g^4 + \cdots\right)\left(1 + p_2 g^2 + p_3 g^3 + p_4 g^4 + \cdots\right)\right\rangle , \tag{9}$$

where the coefficients $w_j$ and $p_j$ are functions of the fields building the Wilson loop and the plaquette respectively. $\langle WP\rangle - \langle W\rangle\langle P_{\mu\nu}(x)\rangle$ can be expressed to the lowest order in terms of $w$ and $p$ as

$$\langle WP_{\mu\nu}(x)\rangle - \langle W\rangle\langle P_{\mu\nu}(x)\rangle = g^4 \left(\langle w_2 p_2\rangle - \langle w_2\rangle\langle p_2\rangle\right) . \tag{10}$$

From (8) one finds that

$$w_2 = \frac{1}{2n} \mathrm{Tr} \sum_{l,m\in W} A_l A_m = \frac{1}{4n} \sum_{l,m\in W} \sum_a A_l^a A_m^a , \tag{11}$$

where the sum is performed over oriented links which means that $A_{-l}$ equals $-A_l$. Identical formula applies for $p_2$ with $\sum_{l,m\in P_{\mu\nu}}$ instead of $\sum_{l,m\in W}$. Deriving (11) we have assumed the representation $A_l = A_l^a T^a$ and standard normalization of the SU(N) generators $\mathrm{Tr}\, T^a T^b = \frac{1}{2}\delta_{ab}$. Now let us consider the term

$$\langle w_2 p_2\rangle = \frac{1}{16n^2} \sum_{l,m\in W} \sum_{l',m'\in P_{\mu\nu}(x)} \sum_{a,a'} \langle A_l^a A_m^a A_{l'}^{a'} A_{m'}^{a'}\rangle . \tag{12}$$

After Wick's expansion of (12) one can complete the subtraction in (10) to obtain

$$\langle W P_{\mu\nu}(x)\rangle - \langle W\rangle\langle P_{\mu\nu}(x)\rangle$$
$$= \frac{g^4}{16n^2} \sum_{l,m\in W} \sum_{l',m'\in P_{\mu\nu}(x)} \sum_{a,a'} \langle A_l^a A_{l'}^{a'}\rangle\langle A_m^a A_{m'}^{a'}\rangle + \langle A_l^a A_{m'}^{a'}\rangle\langle A_m^a A_{l'}^{a'}\rangle$$
$$= \frac{n_g}{2\beta^2} \sum_{l,m\in W} \sum_{l',m'\in P_{\mu\nu}(x)} \varepsilon_{ll'}\varepsilon_{mm'} D(l,l')\, D(m,m')\,, \tag{13}$$

where $\beta = 2n/g_0^2$ , $n_g$ is the number of gluons and equals 3 for SU(2), $\varepsilon_{ll'}$ takes care of the sign (*i.e.* equals $+1$ if the links $l$, $l'$ have the same orientation in $W$ and $P_{\mu\nu}(x)$ and $-1$ if the orientations are opposite). $D(l,l') = D_{\mu(l)\nu(l')}(x_l, x_{l'})$ is the lattice propagator between sites defining the links $l$ , $l'$ . Appropriate formula for $\langle W\rangle$ reads

$$\langle W\rangle = 1 - \frac{n_g}{2\beta} \sum_{l,m\in W} \varepsilon_{lm} D(l,m)\,, \tag{14}$$

but considering only the Born approximation for $f_{\mu\nu}$, we can set $\langle W\rangle = 1$ in (1) obtaining

$$f_{\mu\nu} = \frac{n_g}{2\beta a^4} \sum_{l,m\in W} \sum_{l',m'\in P_{\mu\nu}(x)} \varepsilon_{ll'}\varepsilon_{mm'} D(l,l') D(m,m')\,, \tag{15}$$

This formula will be directly used for numerical studies of the distribution of the chromoelectromagnetic fields in the perturbative domain.

## 3. Implementation

Computations have been carried out on an IBM RISC station. They were split into two main steps: (1) obtaining an array of lattice propagators using Fast Fourier Transform and (2) performing calculations of the correlations required by equation (15). Periodic boundary conditions were used for both steps of computations. The gluonic propagator on a lattice can be expressed as the Fourier Transform of the simple function

$$\overline{D}_{\mu\nu}(p,k) = \delta(p,-k)\delta_{\mu\nu}\frac{1}{\hat{p}\cdot\hat{k}}\,, \tag{16}$$

where $\hat{p}_\rho$ is defined as $\exp(-ip_\rho) - 1$ , so that

$$D_{\mu\nu}(0,m) = \frac{\delta_{\mu\nu}}{V} \sum_p \frac{e^{imp}}{8 - 2\sum_\rho \cos p_\rho}\,, \tag{17}$$

where $V = N_1 \cdot \ldots \cdot N_4$ is the discrete volume of the lattice, $p_\rho = 2\pi k_\rho / N_\rho$, $k_\rho = 0, 1, \ldots, N_\rho - 1$ for the periodic boundary conditions, and the sum over $p$ means summation over all possible $(p_1, p_2, p_3, p_4)$ .

Instead of working out propagators and correlations simultaneously, we performed very efficient 4d FFT computations obtaining once all possible propagators for a particular lattice. It was done by the program performing FFT for any given set of $N_1 \ldots N_4$. Due to the periodic boundary conditions the output file can be quite small and easy for reusing even for large lattices. For example, to obtain the complete set of the propagators for the medium size lattice $16^4$ we have consumed about 20 seconds of the IBM Risc station. The size of the output file was 60 kbytes. Appropriate numbers for the $32^4$ lattice: 60 seconds and 1Mb. Having produced an array of propagators we carried out the correlation calculations using another program producing correlations inside the given volume around the center of the Wilson loop along with cross-sections (applying interpolation if needed). It can be done for any component and given range of sizes of Wilson loops.

## 4. Results

We have performed part of the computations on a $17^3 \cdot 20$ lattice to preserve the possibility of direct comparison with the MC data produced by the Cracow–LSU collaboration. Results from much bigger lattice, *i.e.* $32^4$, were also obtained for more precise study. All computations were carried out for $\beta = 2.4$. Lattice constant is set to unity except in the comparisons with the Monte Carlo results. The Wilson loop lies in the plane *34* and its size is denoted by $R$ (space *i.e.* $z$ direction say) and $T$ (euclidean time, $t$). The center of the loop is located at the origin. Thus, $\pm R/2, \pm T/2$ establish the corners of the loop. All results are presented in terms of four squared components: longitudinal electric/magnetic $E_\parallel^2 = E_z^2$, $B_\parallel^2 = B_z^2$ (plaquettes in planes *34*, *12* respectively) and transverse electric/magnetic $E_\perp^2 = E_x^2 + E_y^2$, $B_\perp^2 = B_x^2 + B_y^2$ (combined from pairs *14*, *24* and *13*, *23* respectively).

As we expect from (15) the $B_\parallel$ (connected with a plaquette in plane *12*) vanishes everywhere (note the presence of the $\delta_{\mu\nu}$ in (17) ). Furthermore, both $B_x$ and $B_y$ vanish in the subspace $t = 0$ (imagine appropriate plaquette lying perpendicularly to the Wilson loop in the same distance from its upper and lower space sides and consider all possible combinations of the $\varepsilon_{ll'}\varepsilon_{mm'}$ in (15) ). Exactly the same observation is true for both $E_x$ and $E_y$ which in turn equals zero if $z = 0$.

These facts result only from the symmetry of the problem and are supported by the numerical computations. They are in agreement with the usual interpretation of the Wilson loop as representing the world line of

the static $q\bar{q}$ pair, giving, in the Born approximation, the fields of a simple electric dipole.

Further results are presented on the following figures. Note: squares, stars *etc.* represent exact, discrete program-produced values. All curves were fitted using slightly corrected spline interpolation method and have only qualitative meaning. Main results concerning the distribution of the fields around quarks are presented in Figs 1–3 for the $32^4$ lattice and $R = 8, T = 11$. They serve mainly as a check of consistency with classical, continuous expectations.

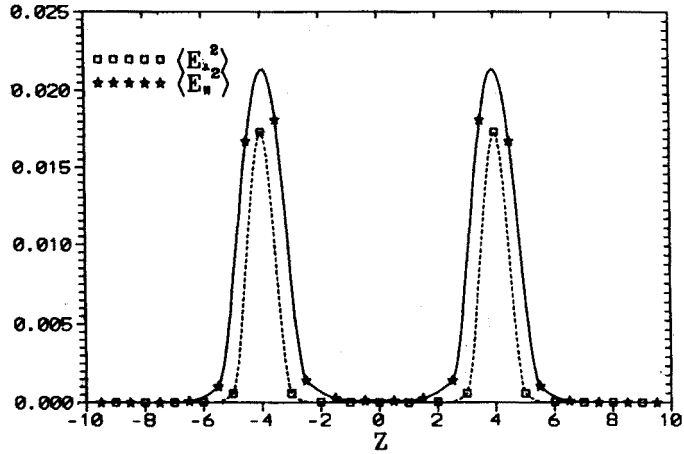


Fig. 1. Longitudinal profiles for $E_{\parallel}^2$ and $E_{\perp}^2$.

Fig. 1 shows typical longitudinal (*i.e.* along $z$ direction ) profiles, for $t = 0$, obtained for the electric longitudinal (stars) and transverse (squares) components respectively. All these profiles are presented for loops with odd $T$ to avoid interpolation in the time direction. Although the produced values for the $E_{\parallel}^2$ lie exactly on the $z$ axis, the appropriate ones for $E_x^2$ do not (effective $x = 1/2$). The classical expectation for $E_x^2$ exactly on the $z$ axis is zero (only longitudinal field exists on a line connecting the charges for the classical electric dipole). Compare results presented in Fig. 2 supporting this expectation. Fig. 1 presents also the most apparent difference between lowest order perturbative and Monte Carlo results: there is practically no field in a large region between quarks *i.e.* no flux tube responsible for confinement. This issue will be discussed below in detail. As was mentioned above there are no magnetic fields at $t = 0$.

Fig. 2 shows the transverse dependence of the $E_x^2$ on the $x$ coordinate for $z = R/2 \pm 3$. Stars represent $R/2 + 3$ and squares $R/2 - 3$. The zero value at $x = 0$ was forced artificially to meet our classical expectation (it

seems not to be very artificial looking at program points). The dashed line lies lower as there is much stronger compensative influence of the quark at $z = -R/2$. Both curves have clear maxima, like appropriate transverse dependence for classical dipole do, and the maximum for the dashed line (inside the dipole) lies at $x$ smaller than that for the solid one (classical maxima: $x_{\max} = 1.83$ for the profile at $z = R/2 - 3$ and $x_{\max} = 2.12$ for $z = R/2 + 3$). It contrasts with the nonperturbative case, where generally fields are stronger between the charges as a result of the flux tube formation and there are no other maxima outside the interquark line.

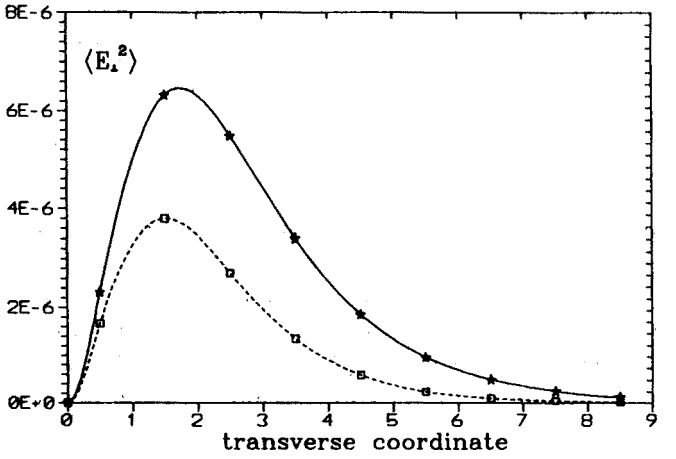


Fig. 2. Transverse dependence for $E_x^2$ and two different $z$.

Transverse dependence for the $E_{\|}^2$ is presented in Fig. 3. The solid, short-dashed and dashed lines are the profiles for $z = R/2 - 0.5$, $z = R/2 - 1.5$ and $z = R/2 - 3.5$ respectively. Again, in agreement with the continuous case, the dependence is monotonic and for every two profiles $z_1, z_2$ one can find such $x$ that these curves cross (although, for instance, the classical crossing point for $z = R/2 - 0.5$ and $z = R/2 - 1.5$ is for $x = 1.27$ and the two lines in the figure meet at $x \approx 2.5$).

The dependence of both nonvanishing magnetic components on $t$ and on the transverse space coordinates for fixed $t$ is generally the same as the one of transverse electric fields on $z$ and $x$ ($y$) for fixed $z$ because of the symmetry $z \leftrightarrow t$, $E \leftrightarrow B$ (exact for square loops). The shape of both energy and action distribution on the $q\bar{q}$ axis is, of course, the same as given in Fig. 1 for $E_{\|}^2$ due to expected vanishing of the $E_{\perp}^2$ and $B^2$.

Now we proceed to the dependence on $T$ for some $q\bar{q}$ separations. We expect that, for any fixed $R$, the components converge to their lowest state values when $T$ gets large. In real measurements based on the MC data,

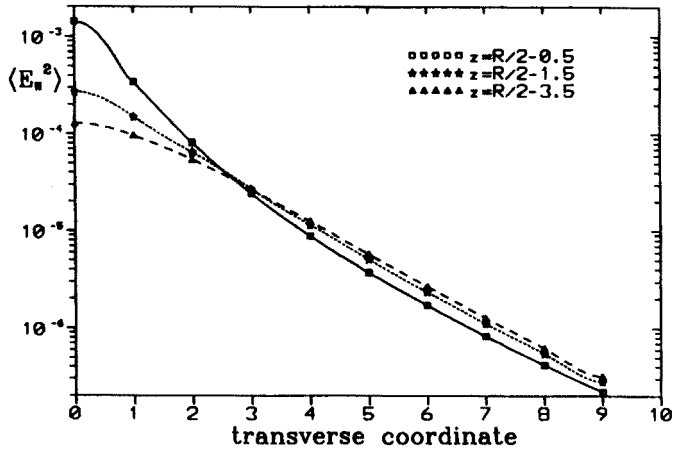


Fig. 3. Transverse dependence for $E_{\parallel}^2$ and various $z$.

the crucial point is how fast the components stabilize *i.e.* for which $T$ the profiles actually describe the lowest state distribution. Also the smoothness of the $T$ dependence is important. We have examined this issue on our data. Up to this point specification of the lattice constant value was not necessary. Now we will set it to the physical value at $\beta = 2.4$ *i.e.* $a = 0.1285$ fm as used in [8] to enable direct comparison with the MC data.

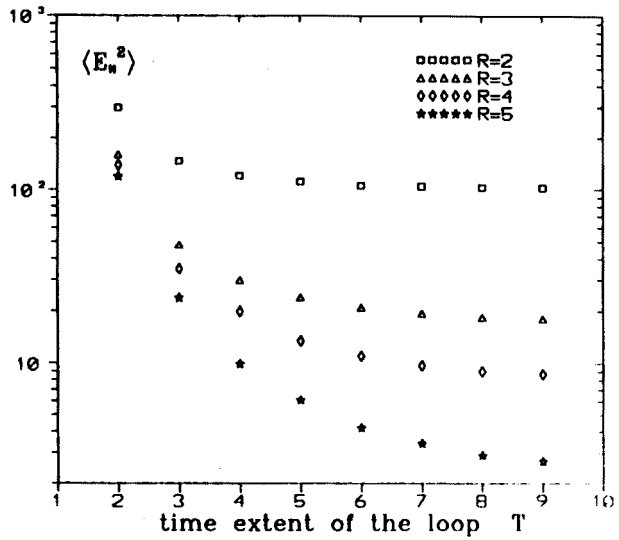


Fig. 4. $E_{\parallel}^2$ at the midpoint between the quarks, $R = 2, 3, 4, 5$.

Fig. 4 presents the $E_{\|}^2$ value at the midpoint between $q$ and $\bar{q}$ and for $t = 0$, as the function of $T$ between 2 and 9 . Note the logarithmic scale on the vertical axis. There are four sets of data points: squares, triangles, diamonds and stars for $R = 2, 3, 4, 5$ respectively. The dependence on $T$ is quite analogous to the one obtained in [8]. The slope is clearly raising with $R$ or, in other words, the values stabilize earlier for smaller $R$ (at $T = 4$ for $R = 2$, $T = 7$ for $R = 3$ and $T = 9$ for $R = 4$). Only for $R = 5$ the stabilization point seems to lie beyond the scope of measured $T$ values (compare similar effect in [8]). Generally, all flux tube profiles presented above are the pure lowest state ones.

The direct comparison of the perturbative vs. Monte Carlo data is shown in Fig. 5. The longitudinal profile for $E_{\|}^2$ for the loop $R = 6, T = 7$ is presented. Squares represent program output points. Monte Carlo data are denoted by stars. This is the direct evidence for nonperturbative and/or higher order perturbative origin of the flux tube between quarks. The effect of forming the tube is in fact much stronger than one can see in this plot as all other components (which vanish in a large area between the charges in the lowest order perturbative limit) have a significant influence in the nonperturbative case. On the other hand, purely perturbative $E_{\|}^2$ is much stronger close to the charges, *i.e.* nonperturbative and/or higher order perturbative effects lower this value. Generally, one can say that turning on these effects results in shifting the significant amount of the energy from the vicinity of the charges to the area between them.

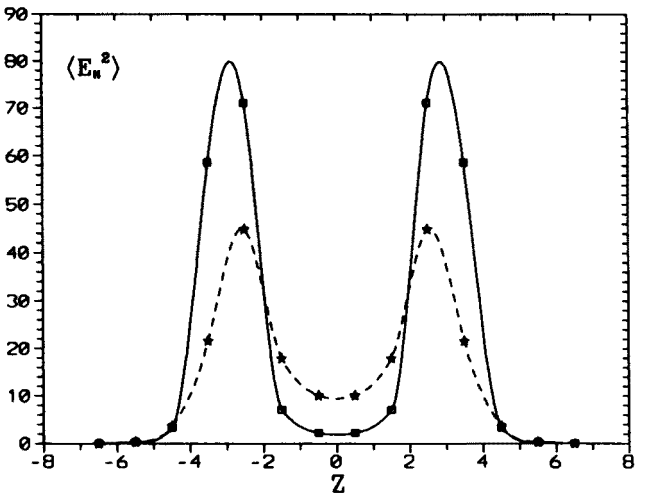


Fig. 5. Perturbative vs. Monte Carlo data: longitudinal profile for $E_{\|}^2$.

## 5. Conclusions

Results presented in this paper confirm that the average values of quantum color fields in the middle of the $q\bar{q}$ system as obtained by lattice MC simulations have nonperturbative and/or higher order perturbative origin. Also the distribution of particular components in the whole space shows clear differences compared to perturbative case: magnetic components have non-zero values in the subspace $t = 0$ and the transverse electric ones do not vanish along the interquark line. There are also some similarities: $E_{\parallel}^2$ is the largest and $B_{\parallel}^2$ the smallest independently of the approach. The dependence of $E_{\parallel}^2$ on $T$ shows similar asymptotic behavior. As one can see, even very simple lowest order calculation can provide useful benchmarks for full nonperturbative results. At the end I would like to stress that performing this study of perturbative fields around static quarks would be very difficult without the help of the FFT method for working out gluonic propagators on the lattice. The algorithm was extended by the author to allow computations on lattices of arbitrary size and asymmetry.

I would like to thank J. Wosiek for suggesting the subject and for numerous discussions.

## REFERENCES

[1] M. Fukugita, T. Niuya, *Phys. Lett.* **132B**, 374 (1983).
[2] J. Flower, S. Otto, *Phys. Lett.* **160B**, 128 (1985).
[3] R. Sommer, *Nucl. Phys.* **B291**, 673 (1987).
[4] J. Wosiek, R.W. Haymaker, *Phys. Rev. Rapid Comm.* **D36**, 3297 (1987).
[5] C. Michael, *Nucl. Phys.* **B280**, 13 (1987).
[6] I.H. Jorysz, C. Michael, *Nucl. Phys.* **B302**, 448 (1987).
[7] R. Sommer, *Nucl. Phys.* **B306**, 180 (1988).
[8] R.W. Haymaker, J. Wosiek, *Acta Phys. Pol.* **B21**, 403 (1990).
[9] R.W. Haymaker, J. Wosiek, *Phys. Rev.* **D43**, 2676 (1991).